Title:

Fibrin biopolymers support recurring mechanical loads by adapting their structure across multiple length scales

Authors:

Nicholas A. Kurniawan,[1,2] Bart E. Vos,[1] Andreas Biebricher,[3] Gijs J. L. Wuite,[3] Erwin J. G. Peterman,[3] and Gijsje H. Koenderink[1,*]

[1]Department of Systems Biophysics, FOM Institute AMOLF, Amsterdam, The Netherlands; [2]Department of Biomedical Engineering & Institute for Complex Molecular Systems, Eindhoven University of Technology, Eindhoven, The Netherlands; and [3]Department of Physics and Astronomy, VU University, Amsterdam, The Netherlands

*Correspondence: g.koenderink@amolf.nl

ABSTRACT

Tissues and cells sustain recurring mechanical loads that span a wide range of loading amplitudes and time scales as a consequence of exposure to blood flow, muscle activity, and external impact. Both tissues and cells derive their mechanical strength from fibrous protein scaffolds, which typically have a complex hierarchical structure. In this study, we take a prototypical example of fibrin, one of the most resilient naturally-occurring biopolymers, which forms the structural scaffold of blood clots. We show how fibrous networks composed of fibrin utilize *irreversible* changes in their hierarchical structure at different scales to maintain *reversible* stress-stiffening up to large strains. To trace the origin of this paradoxical resilience, we systematically tuned the microstructural parameters of fibrin and used a combination of optical tweezers and fluorescence microscopy to measure the interactions of single fibrin fibers for the first time. We demonstrate that fibrin networks adapt to moderate strains by remodeling at the network scale, through spontaneous formation of new bonds between fibers, whereas they adapt to high strains by plastic remodeling of the fibers themselves. This multi-scale adaptation mechanism endows fibrin gels with the remarkable ability to sustain recurring loads due to shear flows and wound stretching. Our findings therefore reveal a microscopic mechanism by which tissues and cells can balance elastic nonlinearity and plasticity that can provide microstructural insights into cell-driven remodeling of tissues.

Keywords: plasticity; nonlinear elasticity; structural hierarchy; optical trapping; fiber network

INTRODUCTION

From a materials perspective, tissues and cells have highly contradictory mechanical properties: they are malleable and adaptive, yet rigid enough to maintain integrity under large mechanical loads (1,2). Studies of a range of natural fibrous materials have identified two general mechanisms that underlie this unusual mechanical functionality. The first is reversible nonlinear stiffening, which allows cells and tissues to increase their resistance to deformation as the applied stress is increased (3,4). This mechanism is observed in a wide variety of biopolymers including actin, collagen, and neurofilaments, and is relatively well-understood in terms of polymer models that predict an intrinsically nonlinear elastic response for networks of stiff fibers (2). The second mechanism instead involves plastic (or inelastic) deformation. Similar to metals, where defects reduce local stresses and slow down cracks (5), Nature effectively utilizes plasticity to toughen cells and tissues against the mechanical demands of their environment (6-8). It is unclear how biomaterials balance elastic nonlinearity and plasticity, especially across the large range of physiological strains encountered throughout the body (9-12).

One characteristic feature of biomaterials that has been speculated to play a crucial role in their mechanical functionality is structural hierarchy (5,13). A paradigmatic example is the extracellular polymer fibrin, which forms networks (Fig. 1 *A*) that consist of fibers (~100 nm diameter) that are themselves bundles of semiflexible protofibrils (~10 nm diameter). Fibrin gels are able to maintain their structural integrity and undergo reversible strain-stiffening up to extraordinarily large strains of close to 300% (14), even though the constituent fibrils undergo changes in molecular structure at tensile strains above ~40% (15). Here we demonstrate that structural adaptation at different length scales underlies fibrin's remarkable mechanical resilience. This intrinsic multi-scale self-adaptation provides a mechanism by which fibrin blood clots can cope with recurring loads due to shear flows and wound stretching. More generally, this mechanism offers a basis for understanding the local and global microstructural remodeling of the extracellular matrix due to cell contractility (16,17) and motility (18,19).

MATERIALS AND METHODS

Fibrin formation and visualization

To form physiological fibrin networks, human fibrinogen (Fib3 in powder form in 20 mM Sodium Citrate-HCl/pH 7.4; Enzyme Research Laboratories, Swansea, UK) was dissolved in water, dialyzed against HBS buffer (20 mM HEPES, 150 mM NaCl, pH 7.4), and polymerized by addition of 1 U/ml human α-thrombin (Enzyme Research Laboratories) and 2 mM $CaCl_2$. To form fibrin networks with minimal bundling, fibrinogen was dialyzed against 50 mM Tris-HCl, 400 mM NaCl, pH 8.5, and polymerized by addition of 0.5 U/ml thrombin and 3.2 mM $CaCl_2$, following Ferry and coworkers (20). Both fibrinogen stocks contain native Factor XIII, as judged by the presence of bands indicating α- and γ-cross-linked chains on reducing SDS-PAGE analysis. To obtain uncross-linked (bundled and unbundled) fibrin networks, 200 μM of D004 inhibitor (Zedira GmBH, Darmstadt, Germany) was added before the initiation of polymerization by

thrombin. The extent of fibrin cross-linking was evaluated using SDS-PAGE as previously described (21). Visualization of hydrated fibrin networks was done using confocal fluorescence microscopy. Unlabeled fibrinogen was mixed with AlexaFluor 488-conjugated fibrinogen (Life Technologies) in a 19:1 molar ratio and polymerized, in the absence or presence of Factor XIII inhibitor, by addition of 0.5 U/ml thrombin for 4 h and at 37°C in sealed glass chambers before imaging. Three-dimensional image stacks were obtained using a confocal laser scanning microscope (Nikon Eclipse Ti, Amsterdam, Netherlands) with a 100× oil immersion objective (NA = 1.49).

Rheometry

Rheological measurements were performed on a stress-controlled rheometer (MCR 501, Anton Paar, Graz, Austria) equipped with a steel cone–plate geometry (1° cone angle, 30 mm diameter). We assembled fibrin samples *in situ* by transferring the fibrinogen solution immediately upon the addition of thrombin onto the preheated (37°C) bottom plate. Solvent evaporation was prevented by coating the sample edges with mineral oil. All measurements were done after 4 h of polymerization.

Dual fiber manipulation

Simultaneous manipulation and visualization of single fibrin fibers were performed using a combined fluorescence microscopy, microfluidics, and quadruple optical tweezers instrument described previously (22,23). Experiments were performed in glass flow cells (Lumicks BV), passivated using 0.2% BSA and 0.5% Pluronic F-127 (Sigma Aldrich), with three laminar (non-mixing) channels. To obtain single fibrin fibers, fibrinogen solution at a concentration of 0.01 mg/ml was polymerized at 37°C by addition of 0.5 U/ml thrombin and transferred to the fibrin channel. Fibrin fibers were captured in the traps with the aid of streptavidin-coated beads (4.5 μm diameter polystyrene microspheres in 0.005% w/v final concentration; Spherotech). Forces on a single bead (bead “A”) were measured by tracking bead displacements using back focal plane interferometry on the trapping laser. For visualization, unlabeled fibrinogen was mixed with AlexaFluor 488-conjugated fibrinogen in a 9:1 molar ratio. Fluorescence excitation was accomplished using a 491 nm laser (Cobolt) in epifluorescence mode. Fluorescence emission was filtered via a dichroic mirror (500/646 dual edge, Semrock) and bandpass filter (540DF80, Chroma), and detected on a cooled EMCCD camera (Photometrics). Fluorescence movies were taken with a 1 second integration time while the force data was simultaneously monitored. Experiments were performed at room temperature. Experiments started under constant flow of the three combined channels (beads, fibrin, HBS buffer) by catching four beads, aligned in pairs along the flow (x-) direction. The beads were then incubated in the fibrin channel until two fibers were caught between each of the bead pairs. The fibers were subsequently moved into the HBS channel, and the flow was stopped. Here, one of the bead pairs (I/II) was first moved in z-direction to bring it below the first bead pair (A/B), then both fibers were positioned orthogonally with respect to each other (I/II aligned in y-direction). Bead pair I/II was subsequently moved upwards until the fibers extended between the two bead pairs made contact (visible as a slight increase in force on bead A). After 10 s, bead pair I/II was moved again downwards. Contact was clearly visible as a force exerted on fiber A/B when the fiber I/II was stretched, concomitant with a visible fiber

bending in the fluorescence image. Stretching was continued until the force expelled one of the beads from the trap (~300 pN).

RESULTS

Plasticity of fibrin

To investigate the (ir)reversibility of the mechanical properties of fibrin networks in response to a wide range of stresses, we use shear rheology and subject fibrin networks to a cyclic logarithmic stress-ramp protocol (Fig. 1 *B*). By ramping up the applied stress from 10^{-1} to 10^{3} Pa, we access strains ranging from 0.1 to 500%. We find that at small maximum stresses, $\tau_{max} < 10$ Pa, the loading and unloading curves closely overlap (Fig. 1 *C*), indicating nearly completely reversible elastic behavior. With higher τ_{max}, however, the unloading curves increasingly deviate from the loading curves. In particular, the network develops a residual strain, γ_{res}, that grows with increasing τ_{max} (Figs. 1, *C* and *F* inset), suggesting an irreversible, inelastic response. Inelastic deformation is typically accompanied by a change in the mechanical properties of the material. To test whether fibrin stiffness is altered by the irreversible deformation, we examine the differential elastic modulus of the network, *K*', during the cyclic loading protocol. Surprisingly, the nonlinear K' vs. applied stress curves for the different cycles fall on top of each other, indicating that the sample stiffness changes reversibly with stress throughout the entire nonlinear strain-stiffening response, even up to stresses close to rupture, both in the increasing (Fig. 1 *D*) and decreasing (Fig. S1 in the Supporting Material) stress ramp cycles. These paradoxical findings of simultaneous *irreversible* deformation and *reversible* nonlinear stress-stiffening are reconciled when we subtract γ_{res} from all the loading curves, resulting in a striking collapse of the data to a single curve (Fig. 1 *F*). Apparently, the network continually adapts to the mechanical loading: the elastic response of deformed and undeformed fibrin networks is indistinguishable, although the sample never returns to the original state (since $\gamma_{res} > 0$). It is important to note that γ_{res} is not a transient viscoelastic effect and does not relax (Fig. S2), consistent with a predominantly elastic behavior (Fig. S3). Moreover, varying the loading and unloading rates marginally affects γ_{res} (Fig. S4). Another notable feature is that smaller stresses are needed in the subsequent loading–unloading cycles to deform the sample to a similar strain level—thus by engineering convention the network softens cyclically—but only for strains up to the maximum strain that the sample has experienced in its history (Fig. 1 *E*). Once the strain exceeds this maximum strain, the loading curve returns to the path that it would have followed in a monotonic stress-ramp test ("virgin path").

Microstructural mechanism of fibrin adaptation

These effects bear a resemblance to the so-called Mullins effect—the observation of residual extension and cyclic softening first seen in natural rubbers (24), which has since been observed in a broad range of materials, including biological tissues and shape-memory alloys (25). However, the cyclic softening in fibrin is milder and happens gradually across the cycles (Fig. S5), in contrast to the sharp softening between the first and second cycles in other materials that exhibit the Mullins effect (26). Although the Mullins-like effect is widely observed, its physical origin appears to be

system-dependent and has been challenging to identify (27). To shed light on this structure–property link, we take a reductionist approach by systematically varying the microstructural parameters of fibrin. Physiological fibrin networks (Fig. 1 *A*) consist of fibers made up of ~65 protofibrils that are both tightly bundled and cross-linked by transglutaminase Factor XIII (21). This cross-linking involves covalent bonds within and between protofibrils (28), thus significantly enhancing the stiffness and elastic limit of the fibers (29), without altering network architecture (Fig. S6 *A*) (21). Adding an inhibitor of FXIII completely abrogates the formation of cross-links (Fig. S6, *B* and *C*). Interestingly, this *uncross-linked* fibrin network (Fig. 2 *A*) also exhibits cyclic softening and a build-up of γ_{res}, but now there is an incomplete return to the virgin path (Fig. 2 *B*). Consequently, the loading curves do not collapse when γ_{res} is subtracted (Fig. 2 *C*), suggesting that the removal of cross-links promotes plastic network deformation.

This irreversible rearrangement can in principle occur either at the level of the network, via formation and dissociation of fiber junctions (30), or at the level of the fibers, via relative slippage between protofibrils and consequent fiber lengthening (26). To test at which structural level plasticity occurs, we examine networks of *unbundled* fibrin fibers, where bundling and therefore protofibril slippage is suppressed (20,31). These networks, referred to as "fine" fibrin clots due to their transparent macroscopic appearance (32), are obtained by a combination of high pH and high salt concentration in the assembly buffer (see Materials and Methods). With an *unbundled* but cross-linked fibrin network (Fig. 2 *D* and Fig. S6), the collapse of the loading curves is restored when we subtract γ_{res} (Fig. 2 *F*), confirming that cross-linking of fibrin fibers, rather than bundling of protofibrils, is responsible for suppressing the plasticity. We finally test *unbundled, uncross-linked* fibrin, and indeed the loading curves do not collapse (Fig. 2, *G–I*). We also notice that at the highest stresses, residual strain values of bundled and unbundled fibrins are very close to each other, regardless of cross-linking (Fig. 2 *J*). Together, these observations indicate that the development of γ_{res} (and therefore irreversibility) arises at the network, rather than fiber, level. An attractive hypothesis to explain this behavior is that network deformation may induce progressive fiber adhesion as fibers align and come closer together during deformation.

Spontaneous fibrin fiber adhesion

To directly test whether fibers can spontaneously associate, we bring individual (bundled and cross-linked) fibers in contact with each other using optical tweezers in conjunction with fluorescence microscopy (23). We employ four traps, each controlling one micrometer-sized bead (22), to catch two fluorescently-labeled single fibrin fibers in a microfluidic channel (see Methods), manipulate them, and measure the interactions between them (Fig. 3 *A*). When we bring the fibers together in an orthogonal configuration, we indeed find that they readily adhere to each other (Fig. 3 *B*). This spontaneous adhesion is easily discernible as bending of one of the fibers when the other is moved (see also Fig. S7, Movies S1 and S2), and it occurs in all fiber pairs we tested (n = 29). Further lateral and vertical manipulations of the fibers do not lead to rupture of the newly-formed fiber junctions, and in all experiments we lost the beads from the trap (at forces of 343 ± 104 pN; see representative force traces in Figs. 3 *C* and S7) with the junction still intact. This finding demonstrates for the first time that upon contact, fibrin fibers rapidly adhere to each other and form a stable adhesion. Spontaneous adhesion between fibers during network deformation can be a physical mechanism by which fibrin structurally adapts to mechanical loads, thereby effectively rearranging network topology and redistributing the stress. If true, then network adaption should be directional: the response should differ in the direction of loading and in the

opposite direction. To test this, we subject fibrin network to asymmetric loadings and indeed find correspondingly asymmetric network adaptation (Fig. S8), consistent with a recent large amplitude oscillatory shear study (26). Taken together, these findings imply a network-level structural adaptation in response to an applied deformation. We speculate that such passive self-adaptation may be important as a rapid physiological response to prevent damage in blood clots, where bundling and aligning of fibers due to blood flow have been observed (33).

Deformational regimes of fibrin

The microscopic irreversibility in the form of spontaneous bond formation that we propose should manifest itself at the macroscopic level in the form of mechanical energy dissipation. To test this hypothesis, we examine rheological signatures of elastic, viscous, and plastic behaviors as a function of the applied stress. First, we look at tan δ, which provides a measure of the importance of viscous dissipation in the form of a ratio between the differential viscous and elastic moduli, K" and K' respectively. Interestingly, tan δ remains constant quite far beyond the linear viscoelastic regime, only starting to increase when the stress reaches values of ~100 Pa, almost two orders of magnitude larger than the onset of stiffening at a critical stress of ~2 Pa (Fig. 4 *B*). Consistent with this, stress-induced viscous flow as quantified by the creep rate $d\gamma/dt$ (Fig. 4 *D* and Fig. S9) also remains negligibly small until the stress reaches 100 Pa. Since the same increase in tan δ and $d\gamma/dt$ is also observed (but with significantly larger magnitude) in uncross-linked fibrin (Fig. S10), we conclude that it reflects viscous dissipation due to structural rearrangement at the network level, mediated by fiber associations (Fig. 4 *A*, left). When the stress reaches values close to the rupture point (>2,000 Pa, corresponding to strains near 200%), we observe a downturn in tan δ. As our previous work has established that this large-stress regime is governed by enthalpic stretching of individual fibers (34), the dissipative mechanism in this regime is likely dominated by remodeling *within* the fibers (Fig. 4 *A*, right). Interestingly, the downturn of tan δ is accompanied by a clear upturn of K' in cross-linked networks (Fig. 4 *B*), whereas uncross-linked networks show a much less pronounced upturn of K' (Fig. S10). Taken together, these findings show that fibrin's extreme elastic resilience originates from network remodeling at intermediate stresses followed by fiber remodeling at higher levels of stress.

Fibrin failure

The remarkable multiscale plasticity of fibrin raises an important question: how does fibrin fail? In general, little is known about the failure modes of biopolymer networks (35), including fibrin. To access fibrin's response close to rupture, we turn to a cyclic logarithmic *strain*-ramp protocol (Fig. 4 *F*), which allows us to carefully approach and exceed the breaking limit without immediately causing failure of the whole sample. We find that in each cycle, a *negative* stress, $\tau_0 < 0$, is needed to bring the sample back to zero strain. Moreover, τ_0 becomes more negative with increasing maximum strain, γ_{max}, just as γ_{res} builds up with increasing τ_{max} in the stress ramp protocol. This finding further supports the hypothesis that the fibrin network continually reconfigures itself. At strains larger than ~100%, the stress needed to achieve γ_{max} suddenly decreases, indicating the onset of sample failure. This failure strain is comparable to that of whole blood clots, which rupture at shear strains of 50–70% depending on hematocrit level (36). Surprisingly, the return-to-virgin-path behavior still persists, even for very large γ_{max} (up to ~1000%). Moreover, both cross-linked and uncross-linked networks exhibit this large-strain

return-to-virgin-path (Fig. 4 *G* and Fig. S11 *A*), indicating that fiber cross-linking and bundling play a negligible role in the rupture mechanics. SDS-PAGE analysis of the ruptured network reveals that, at the molecular level, the cross-links are not disrupted by sample failure (Fig. S11 *C*). These results strongly suggest a gradual and progressive rupture at the *network* level (as opposed to the fiber or protofibril level), where the structure that survives the previous deformation step is still intact and is only perturbed when the sample is stretched to even larger deformations, resulting in 'damage' propagation. To check whether plastic remodeling still occurs during this damage propagation, we plot τ_0 as a function of γ_{max}. We indeed find that, beyond 100% strain, τ_0 no longer decreases, confirming the absence of significant network reconfiguration (Fig. 4 *H* and Fig. S11 *B*).

DISCUSSION

The mechanical resilience of fibrin has been ascribed to its nonlinear elastic behavior, which allows fibrin networks to stiffen as they are increasingly deformed. Previous studies from our group have shown that fibrin's characteristic nonlinear stiffening derives from its structural hierarchy (34), with network entropic stiffening dominating at small stresses and fiber enthalpic stiffening dominating at large stresses (21,31). While these elastic effects are relatively well-understood, fibrin's viscoplastic behavior in response to recurring mechanical loads has been largely overlooked. Our current work demonstrates that fibrin networks exhibit a surprising combination of plasticity in the form of *irreversible* structural adaptation at different scales with *reversible* stress-stiffening, and that it is this mechanism that endows them with an extensive mechanical resilience. Under small deformations, fibrin behaves predominantly elastically with a small degree of irreversibility, as manifested in the development of residual strains. Increasing amounts of deformation lead to increasing irreversibility. By systematically dissecting the contributions of network cross-linking and fiber bundling to network viscoplasticity together with dual-fiber manipulations by optical tweezers, we show that plasticity is operative at the network (instead of fiber) level via spontaneous formation of new bonds. This network remodeling ensures a reversible stress-stiffening response with no apparent change in the modulus. At large deformations, plasticity is operative at the molecular scale within the fibers: the fibers themselves remodel to dissipate mechanical energy. One possible effect of this fiber-level remodeling is force-induced lengthening of individual fibrin fibers, which has been reported by Münster *et al* (26). Beyond this point, the network response and failure are governed by progressive damage propagation.

Our results raise three important questions. First, what is the molecular basis for the spontaneous adhesion of fibrin fibers? A recent high-resolution atomic force microscopy study revealed that the surface of fibrin protofibrils and fibers is covered by a hairy coat of unstructured αC chain protrusions (37). Since these peptide chains are known to self-associate into polymers via a β-hairpin swapping mechanism (38), forming bonds with a rupture strength of ~50 pN that are further reinforced by covalent, FXIII-mediated cross-linking (39), we speculate that they are likely responsible for the spontaneous formation of stable fiber–fiber contacts in a Velcro-like adhesion. It will be interesting to test this idea using molecular dynamics simulations, building on recent progress in modeling the structure and interactions of fibrinogen (40,41). In addition to

providing insight into the molecular basis of the structural adaptation of blood clots under mechanical load, addressing this question can potentially contribute to devising a molecular tool for tuning the stickiness of fibrin glues and sealants that are widely used in surgeries and regenerative medicine (42,43). A second question raised by our findings is whether other fibrous biopolymer networks can also benefit from this self-adhesion mechanism to extend their reversible strain-stiffening response. In particular, intracellular intermediate filaments and extracellular collagen fibers are known to exhibit a hierarchy of quaternary structures including fiber bundling and to strain-stiffen reversibly (2) up to strains close to 300% in case of intermediate filaments (44) and 50% in case of collagen (45,46). It will be interesting to extend our quadruple optical tweezer assay to measure the interactions between single intermediate filaments or collagen fibers. The third question raised by our data concerns the molecular mechanism of fiber remodeling that occurs at large stresses, especially in unbundled fibrin networks. There is already evidence of force-induced conformational changes (47) and unfolding of fibrin monomers (15) under mechanical loading, which may be responsible for the dissipative remodeling. Here coarse-grained simulations are likely needed to connect molecular-scale insights from full-atom simulations to macroscale mechanics at the protofibril and fiber levels.

Cells (48), cytoskeletal components including actin networks (49), and extracellular matrix components such as collagen networks (26,46,50) have been shown to exhibit some degree of plasticity in response to recurring mechanical loading, although the structural origins are still not fully understood. The mechanistic link between the macroscopic mechanics of biopolymer networks and the underlying microscopic mechanisms of remodeling that our work offers can provide a basis to better understand the microstructural principles behind cell-driven plastic reshaping of tissues in wound healing (51), during organogenesis in embryo development (52), and in tissue engineering (53). More generally, the multi-scale interplay between elasticity and plasticity that we identified here in a prototypical hierarchical biomaterial opens the possibility for the rational design of synthetic materials and hydrogels that mimic the extreme toughness and flexibility of living matter (54,55). An attractive approach is to incorporate dynamic covalent bonds (56) or a judicious balance of hydrophilic and hydrophobic moieties (57) into hierarchically self-assembling peptides (58) to achieve stimuli-responsive remodeling at multiple structural length scales.

SUPPORTING MATERIAL

Eleven figures and two movies are available at ….

AUTHOR CONTRIBUTIONS

N.A.K. and G.H.K. conceived the research. N.A.K. performed rheology, microscopy, and SDS-PAGE experiments. N.A.K., B.E.V., and A.B. performed quadruple optical tweezers experiments. A.B., G.J.L.W., and E.J.G.P. provided expertise on analyzing the optical tweezers data. N.A.K., B.E.V., and G.H.K. wrote the manuscript. All authors revised the manuscript.

ACKNOWLEDGMENTS

The authors thank J. Grimbergen and J. Koopman for providing Factor XIII inhibitor; A. Candelli, B.M. Mulder, M. Vahabi, L. Liebrand, F.C. MacKintosh, and K.A. Jansen for insightful discussions; and M. van Hecke for critical reading of the manuscript.

This work is part of the research programme of the Foundation for Fundamental Research on Matter (FOM), which is part of the Netherlands Organisation for Scientific Research (NWO). N.A.K. acknowledges support from a Marie Curie IIF fellowship.

Quadruple optical trap technology is licensed by VU University Amsterdam to LUMICKS B.V., of which G.J.L.W. and E.J.G.P. are co-owners. All other authors declare no competing financial interests.

REFERENCES

1. Roh-Johnson, M., G. Shemer, C. D. Higgins, J. H. McClellan, A. D. Werts, U. S. Tulu, L. Gao, E. Betzig, D. P. Kiehart, and B. Goldstein. 2012. Triggering a cell shape change by exploiting preexisting actomyosin contractions. Science 335:1232-1235.
2. Storm, C., J. J. Pastore, F. C. MacKintosh, T. C. Lubensky, and P. A. Janmey. 2005. Nonlinear elasticity in biological gels. Nature 435:191-194.
3. Fung, Y.-C. 1993. Biomechanics: Mechanical Properties of Living Tissues. Springer-Verlag, New York.
4. Fernández, P., P. A. Pullarkat, and A. Ott. 2006. A master relation defines the nonlinear viscoelasticity of single fibroblasts. Biophys. J. 90:3796-3805.
5. Weinkamer, R., J. W. C. Dunlop, Y. Bréchet, and P. Fratzl. 2013. All but diamonds – Biological materials are not forever. Acta Mater. 61:880-889.
6. Wegst, U. G., H. Bai, E. Saiz, A. P. Tomsia, and R. O. Ritchie. 2015. Bioinspired structural materials. Nature Mater. 14:23-36.
7. Gralka, M., and K. Kroy. 2015. Inelastic mechanics: A unifying principle in biomechanics. Biochim. Biophys. Acta 1853:3025-3037.
8. Kurniawan, N. A., P. K. Chaudhuri, and C. T. Lim. 2016. Mechanobiology of cell migration in the context of dynamic two-way cell–matrix interactions. J. Biomech. 49:1355-1368.
9. Buehler, M. J., and Y. C. Yung. 2009. Deformation and failure of protein materials in physiologically extreme conditions and disease. Nature Mater. 8:175-188.
10. Schwarz, U. S., and S. A. Safran. 2013. Physics of adherent cells. Rev. Mod. Phys. 85:1327-1381.
11. Klotzsch, E., M. L. Smith, K. E. Kubow, S. Muntwyler, W. C. Little, F. Beyeler, D. Gourdon, B. J. Nelson, and V. Vogel. 2009. Fibronectin forms the most extensible biological fibers displaying switchable force-exposed cryptic binding sites. Proc. Natl. Acad. Sci. USA 106:18267-18272.
12. Guan, J., D. Porter, and F. Vollrath. 2012. Silks cope with stress by tuning their mechanical properties under load. Polymer 53:2717-2726.
13. Meyers, M. A., J. McKittrick, and P. Y. Chen. 2013. Structural biological materials: critical mechanics-materials connections. Science 339:773-779.

14. Brown, A. E. X., R. I. Litvinov, D. E. Discher, P. K. Purohit, and J. W. Weisel. 2009. Multiscale mechanics of fibrin polymer: Gel stretching with protein unfolding and loss of water. Science 325:741-744.
15. Zhmurov, A., O. Kononova, R. I. Litvinov, R. I. Dima, V. Barsegov, and J. W. Weisel. 2012. Mechanical transition from α-helical coiled coils to β-sheets in fibrin(ogen). J. Am. Chem. Soc. 134:20396-20402.
16. Jansen, K. A., R. G. Bacabac, I. K. Piechocka, and G. H. Koenderink. 2013. Cells actively stiffen fibrin networks by generating contractile stress. Biophys. J. 105:2240-2251.
17. Wong, L. H., N. A. Kurniawan, H.-P. Too, and R. Rajagopalan. 2014. Spatially resolved microrheology of heterogeneous biopolymer hydrogels using covalently bound microspheres. Biomech. Model. Mechanobiol. 13:839-849.
18. Sun, W., N. A. Kurniawan, A. P. Kumar, R. Rajagopalan, and C. T. Lim. 2014. Effects of migrating cell-induced matrix reorganization on 3D cancer cell migration. Cell. Mol. Bioeng. 7:205-217.
19. Bloom, R. J., J. P. George, A. Celedon, S. X. Sun, and D. Wirtz. 2008. Mapping local matrix remodeling induced by a migrating tumor cell using three-dimensional multiple-particle tracking. Biophys. J. 95:4077-4088.
20. Bale, M. D., M. F. Muller, and J. D. Ferry. 1985. Effects of fibrinogen-binding tetrapeptides on mechanical properties of fine fibrin clots. Proc. Natl. Acad. Sci. USA 82:1410-1413.
21. Kurniawan, N. A., J. Grimbergen, J. Koopman, and G. H. Koenderink. 2014. Factor XIII stiffens fibrin clots by causing fiber compaction. J. Thromb. Haemost. 12:1687-1696.
22. Laurens, N., R. P. C. Driessen, I. Heller, D. Vorselen, M. C. Noom, F. J. H. Hol, M. F. White, R. T. Dame, and G. J. L. Wuite. 2012. Alba shapes the archaeal genome using a delicate balance of bridging and stiffening the DNA. Nature Commun. 3:1328.
23. van Mameren, J., M. Modesti, R. Kanaar, C. Wyman, E. J. Peterman, and G. J. Wuite. 2009. Counting RAD51 proteins disassembling from nucleoprotein filaments under tension. Nature 457:745-748.
24. Mullins, L. 1969. Softening of rubber by deformation. Rubber Chem. Technol. 42:339-362.
25. Schmoller, K. M., and A. R. Bausch. 2013. Similar nonlinear mechanical responses in hard and soft materials. Nature Mater. 12:278-281.
26. Münster, S., L. M. Jawerth, B. A. Leslie, J. I. Weitz, B. Fabry, and D. A. Weitz. 2013. Strain history dependence of the nonlinear stress response of fibrin and collagen networks. Proc. Natl. Acad. Sci. USA 110:12197-12202.
27. Diani, J., B. Fayolle, and P. Gilormini. 2009. A review on the Mullins effect. Eur. Polym. J. 45:601-612.
28. Ariëns, R. A. S., T. S. Lai, J. W. Weisel, C. S. Greenberg, and P. J. Grant. 2002. Role of factor XIII in fibrin clot formation and effects of genetic polymorphisms. Blood 100:743-754.
29. Helms, C. C., R. A. Ariens, S. Uitte de Willige, K. F. Standeven, and M. Guthold. 2012. α-α Cross-links increase fibrin fiber elasticity and stiffness. Biophys. J. 102:168-175.
30. Carlisle, C. R., E. A. Sparks, C. Der Loughian, and M. Guthold. 2010. Strength and failure of fibrin fiber branchpoints. J. Thromb. Haemost. 8:1135-1138.
31. Piechocka, I. K., K. A. Jansen, C. P. Broedersz, N. A. Kurniawan, F. C. MacKintosh, and G. H. Koenderink. 2016. Multi-scale strain-stiffening of semiflexible bundle networks. Soft Matter 12:2145-2156.

32. Ferry, J. D., and P. R. Morrison. 1947. Preparation and properties of serum and plasma proteins. VIII. The conversion of human fibrinogen to fibrin under various conditions. J. Am. Chem. Soc. 69:388-400.
33. Whittaker, P., and K. Przyklenk. 2009. Fibrin architecture in clots: A quantitative polarized light microscopy analysis. Blood Cell. Mol. Dis. 42:51-56.
34. Piechocka, I. K., R. G. Bacabac, M. Potters, F. C. MacKintosh, and G. H. Koenderink. 2010. Structural hierarchy governs fibrin gel mechanics. Biophys. J. 98:2281-2289.
35. Jung, G., Z. Qin, and M. J. Buehler. 2015. Mechanical properties and failure of biopolymers: atomistic reactions to macroscale response. Top. Curr. Chem. 369:317-343.
36. Riha, P., X. Wang, R. Liao, and J. F. Stoltz. 1999. Elasticity and fracture strain of whole blood clots. Clin. Hemorheol. Microcirc. 21:45-49.
37. Protopopova, A. D., N. A. Barinov, E. G. Zavyalova, A. M. Kopylov, V. I. Sergienko, and D. V. Klinov. 2015. Visualization of fibrinogen αC regions and their arrangement during fibrin network formation by high-resolution AFM. J. Thromb. Haemost. 13:570-579.
38. Tsurupa, G., I. Pechik, R. I. Litvinov, R. R. Hantgan, N. Tjandra, J. W. Weisel, and L. Medved. 2012. On the mechanism of αC polymer formation in fibrin. Biochemistry 51:2526-2538.
39. Litvinov, R. I., S. Yakovlev, G. Tsurupa, O. V. Gorkun, L. Medved, and J. W. Weisel. 2007. Direct evidence for specific interactions of the fibrinogen αC-domains with the central E region and with each other. Biochemistry 46:9133-9142.
40. Kononova, O., R. I. Litvinov, A. Zhmurov, A. Alekseenko, C. H. Cheng, S. Agarwal, K. A. Marx, J. W. Weisel, and V. Barsegov. 2013. Molecular mechanisms, thermodynamics, and dissociation kinetics of knob-hole interactions in fibrin. J. Biol. Chem. 288:22681-22692.
41. Kohler, S., F. Schmid, and G. Settanni. 2015. The internal dynamics of fibrinogen and its implications for coagulation and adsorption. PLoS Comp. Biol. 11:e1004346.
42. Rousou, J. A. 2013. Use of fibrin sealants in cardiovascular surgery: A systematic review. J. Card. Surg. 28:238-247.
43. Janmey, P. A., J. P. Winer, and J. W. Weisel. 2009. Fibrin gels and their clinical and bioengineering applications. J. R. Soc. Interface 6:1-10.
44. Yao, N. Y., C. P. Broedersz, Y. C. Lin, K. E. Kasza, F. C. Mackintosh, and D. A. Weitz. 2010. Elasticity in ionically cross-linked neurofilament networks. Biophys. J. 98:2147-2153.
45. Sharma, A., A. J. Licup, K. A. Jansen, R. Rens, M. Sheinman, G. H. Koenderink, and F. C. MacKintosh. 2016. Strain-controlled criticality governs the nonlinear mechanics of fibre networks. Nature Phys.:in press.
46. Kurniawan, N. A., L. H. Wong, and R. Rajagopalan. 2012. Early stiffening and softening of collagen: interplay of deformation mechanisms in biopolymer networks. Biomacromolecules 13:691-698.
47. Litvinov, R. I., D. A. Faizullin, Y. F. Zuev, and J. W. Weisel. 2012. The α-helix to β-sheet transition in stretched and compressed hydrated fibrin clots. Biophys. J. 103:1020-1027.
48. Fernandez, P., and A. Ott. 2008. Single cell mechanics: Stress stiffening and kinematic hardening. Phys. Rev. Lett. 100:238102.
49. Schmoller, K. M., P. Fernandez, R. C. Arevalo, D. L. Blair, and A. R. Bausch. 2010. Cyclic hardening in bundled actin networks. Nature Commun. 1:134.
50. Nam, S., K. H. Hu, M. J. Butte, and O. Chaudhuri. 2016. Strain-enhanced stress relaxation impacts nonlinear elasticity in collagen gels. Proc. Natl. Acad. Sci. USA 113:5492-5497.
51. Wong, V. W., S. Akaishi, M. T. Longaker, and G. C. Gurtner. 2011. Pushing back: wound mechanotransduction in repair and regeneration. J. Invest. Dermatol. 131:2186-2196.

52. Miller, C. J., and L. A. Davidson. 2013. The interplay between cell signalling and mechanics in developmental processes. Nat. Rev. Genet. 14:733-744.
53. Williams, G. M., J. W. Lin, and R. L. Sah. 2007. Cartilage reshaping via in vitro mechanical loading. Tissue Eng. 13:2903-2911.
54. Sun, J. Y., X. Zhao, W. R. Illeperuma, O. Chaudhuri, K. H. Oh, D. J. Mooney, J. J. Vlassak, and Z. Suo. 2012. Highly stretchable and tough hydrogels. Nature 489:133-136.
55. Jaspers, M., M. Dennison, M. F. Mabesoone, F. C. MacKintosh, A. E. Rowan, and P. H. Kouwer. 2014. Ultra-responsive soft matter from strain-stiffening hydrogels. Nature Commun. 5:5808.
56. Ying, H., Y. Zhang, and J. Cheng. 2014. Dynamic urea bond for the design of reversible and self-healing polymers. Nature Commun. 5:3218.
57. Phadke, A., C. Zhang, B. Arman, C. C. Hsu, R. A. Mashelkar, A. K. Lele, M. J. Tauber, G. Arya, and S. Varghese. 2012. Rapid self-healing hydrogels. Proc. Natl. Acad. Sci. USA 109:4383-4388.
58. O'Leary, L. E., J. A. Fallas, E. L. Bakota, M. K. Kang, and J. D. Hartgerink. 2011. Multi-hierarchical self-assembly of a collagen mimetic peptide from triple helix to nanofibre and hydrogel. Nature Chem. 3:821-828.

Figure legends

FIGURE 1 Elasticity and plasticity in fibrin networks. (*A*) Representative confocal image (left; maximum intensity projection of 25.6 μm stack; scale bar = 10 μm) of 2 mg/ml physiological (i.e., bundled and cross-linked) fibrin network ("WT") and a schematic representation of the cross-linked, bundled fiber architecture (right). (*B*) Cyclic logarithmic stress ramp protocol. (*C*) The stress–strain response of 2 mg/ml fibrin network (in log scale), showing the accumulation of residual strain, γ_{res}, after each cycle. The color coding corresponds to that of the protocol in (*B*), with solid lines indicating increasing applied stress and dashed lines indicating decreasing stress. The corresponding stress–strain response of a 4% polyacrylamide gel is also shown for comparison, showing the complete reversibility of the response and the lack of any residual strain. (*D*) Despite the development in the (plastic) residual strain, γ_{res}, the fibrin network continues to exhibit reversible stress-stiffening. The differential elastic modulus, $K' = d\tau/d\gamma$, is plotted as a function of stress, τ, for the loading part of each cycle (different colors), showing that all curves overlap. Arrows indicate the maximum stresses reached, τ_{max}, in each cycle, with corresponding color coding. (*E*) A zoom-in of two loading curves from (*C*), highlighting the return-to-virgin-path behavior. (*F*) When γ_{res} is substracted from each loading curve in *C*, all curves collapse, indicating that, despite the large residual strain, the network mechanically behaves exactly like an undeformed, virgin network. The γ_{res} is shown in the inset as a function of the largest stress that the sample has been subjected to.

FIGURE 2 Microstructural basis of fibrin network plasticity. We probe the microstructural origin of fibrin's plasticity by examining networks of (*A–C*) uncross-linked fibrin (xl^-), (*D–F*) unbundled fibrin fibers (bnd^-), and (*G–I*) unbundled and uncross-linked fibrin fibers (bnd^-/xl^-). Schematic representations for the three networks are shown in (*A*), (*D*), and (*G*), and the corresponding stress–strain responses to a cyclic logarithmic shear protocol are shown in (*B*), (*E*), and (*H*). The complete return to virgin path is not observed in the uncross-linked bundled (*B*) nor uncross-linked unbundled (*H*) fibrin networks, as indicated by the arrows. After γ_{res} subtraction, the curves collapse for the unbundled fibrin network (*F*), but not for the uncross-linked, bundled (*C*) or unbundled (*I*), networks. The progression of γ_{res} with τ_{max} is plotted in (*J*), with that for the physiologically relevant situation (i.e., bundled and cross-linked) fibrin network (WT) also shown.

FIGURE 3 Direct evidence for spontaneous lateral association between fibrin fibers. Two fibrin fibers are captured using two pairs of beads that are trapped using optical tweezers. The first fiber is fixed in place by trapping beads A and B, while the second is moved around by positioning beads I and II. (*A*) and (*B*) respectively show inverted fluorescence intensity images and three-dimensional schematic representations of the fibers labeled with AlexaFluor488 and beads. Circles outline the positions of the beads, with dashed outlines indicating out-of-focus beads. (*C*) shows the corresponding force responses on bead A. After the two fibers are captured (1), one of them (held by bead pair I/II) is moved vertically downward (i.e., out of plane) (2) and then brought up again to touch the other fiber in an orthogonal configuration (3). Lateral association between the two fibers is spontaneously established, as indicated by the bending of the second fiber and the increase in the force on bead A when the first fiber is moved in-plane (4) or vertically (5).

FIGURE 4 Structural adaption of cross-linked, bundled fibrin networks at different scales across different deformational regimes. (*A*) A schematic model describing fibrin's structural adaptations at the network (1 and 2) and fiber (3 and 4) levels in response to increasing applied stress. Intermediate levels of stress leads to remodeling at the network level, exemplified by spontaneous fiber adhesion during deformation (1 → 2), whereas large levels of stress results in internal remodeling within the fibers, as depicted by the stretching of the individual protofibrils (3 → 4). At the macroscopic level, these adaptations manifest as distinct stress-dependent mechanical regimes (*B*–*E*). (*B*) The differential elastic modulus, *K*', which reports the effective stiffness at different levels of stress, (*C*) tan δ, which reports the ratio between viscous *K*" and elastic *K*' moduli, (*D*) creep rate ($\mathrm{d}\gamma/\mathrm{dt}$), which reports the propensity of the samples to flow, and (*E*) residual strain (γ_{res}), a measure of plastic remodeling, are plotted as a function of the applied stress. Creep rate is obtained from the time derivative of the creep response to step changes in applied stress (see Fig. S9). To probe the extreme limit of plasticity (5), we used a strain-controlled cyclic logarithmic protocol (*F*). The stress–strain response to this protocol is plotted in (*G*), showing that, surprisingly, mechanical memory is still retained even after network rupture, as indicated by the return to virgin path (*arrow heads*) beyond the maximum stress. Negative stresses τ_0 are needed to bring the networks back to zero strain after each deformation cycle (*H*). The magnitude of τ_0 gradually increases with the maximum applied strain, γ_{max}, but reaches a plateau when the network ruptures. Dashed lines are to guide the eye.

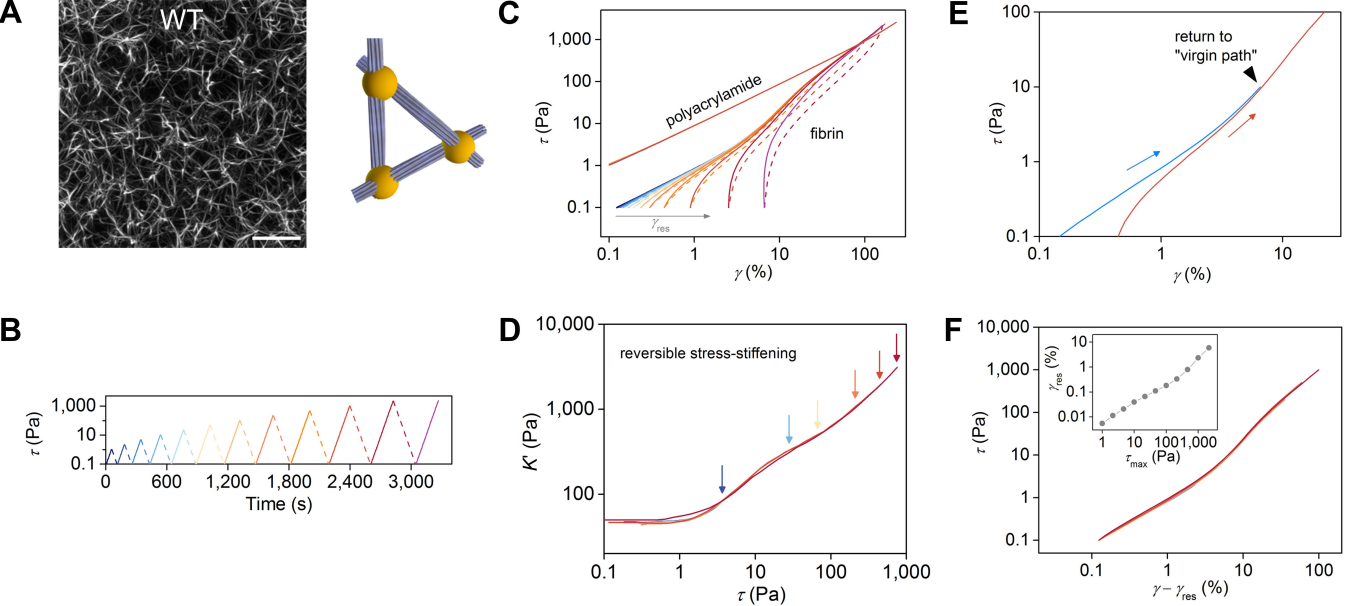
A
WT
B
τ (Pa)
1,000
10
0.1
0
600
1,200
1,800
2,400
3,000
Time (s)
C
1,000
100
10
1
0.1
τ (Pa)
polyacrylamide
fibrin
γres
0.1
1
10
100
γ (%)
D
10,000
1,000
100
K' (Pa)
reversible stress-stiffening
0.1
1
10
100
1,000
τ (Pa)
E
100
10
1
0.1
τ (Pa)
return to
"virgin path"
0.1
1
10
γ (%)
F
10,000
1,000
100
10
1
0.1
τ (Pa)
γres (%)
10
1
0.1
0.01
1
10
100
1,000
τmax (Pa)
0.1
1
10
100
γ − γres (%)

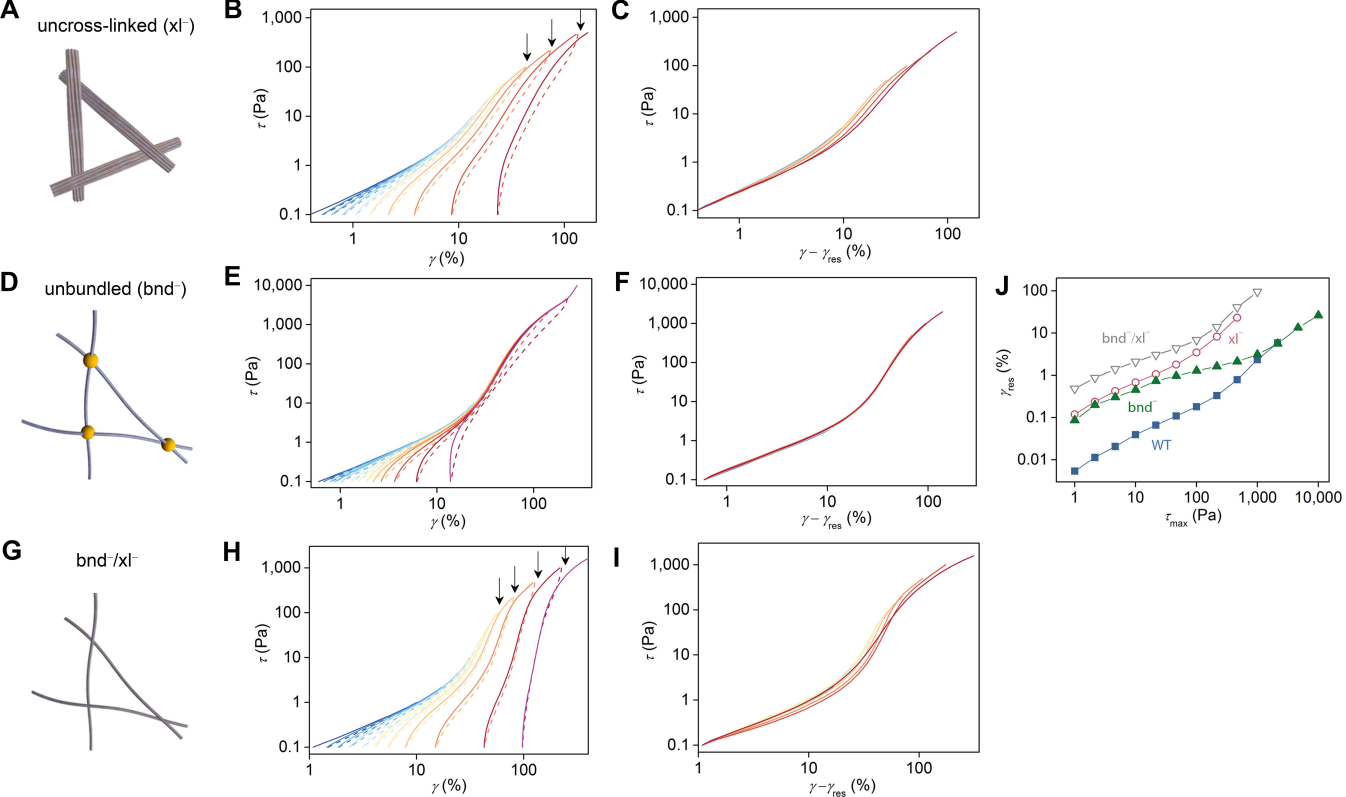
A
uncross-linked (xl⁻)
B
C
D
unbundled (bnd⁻)
E
F
J
G
bnd⁻/xl⁻
H
I
τ (Pa)
γ (%)
γ − γres (%)
γres (%)
τmax (Pa)
bnd⁻/xl⁻
xl⁻
bnd⁻
WT

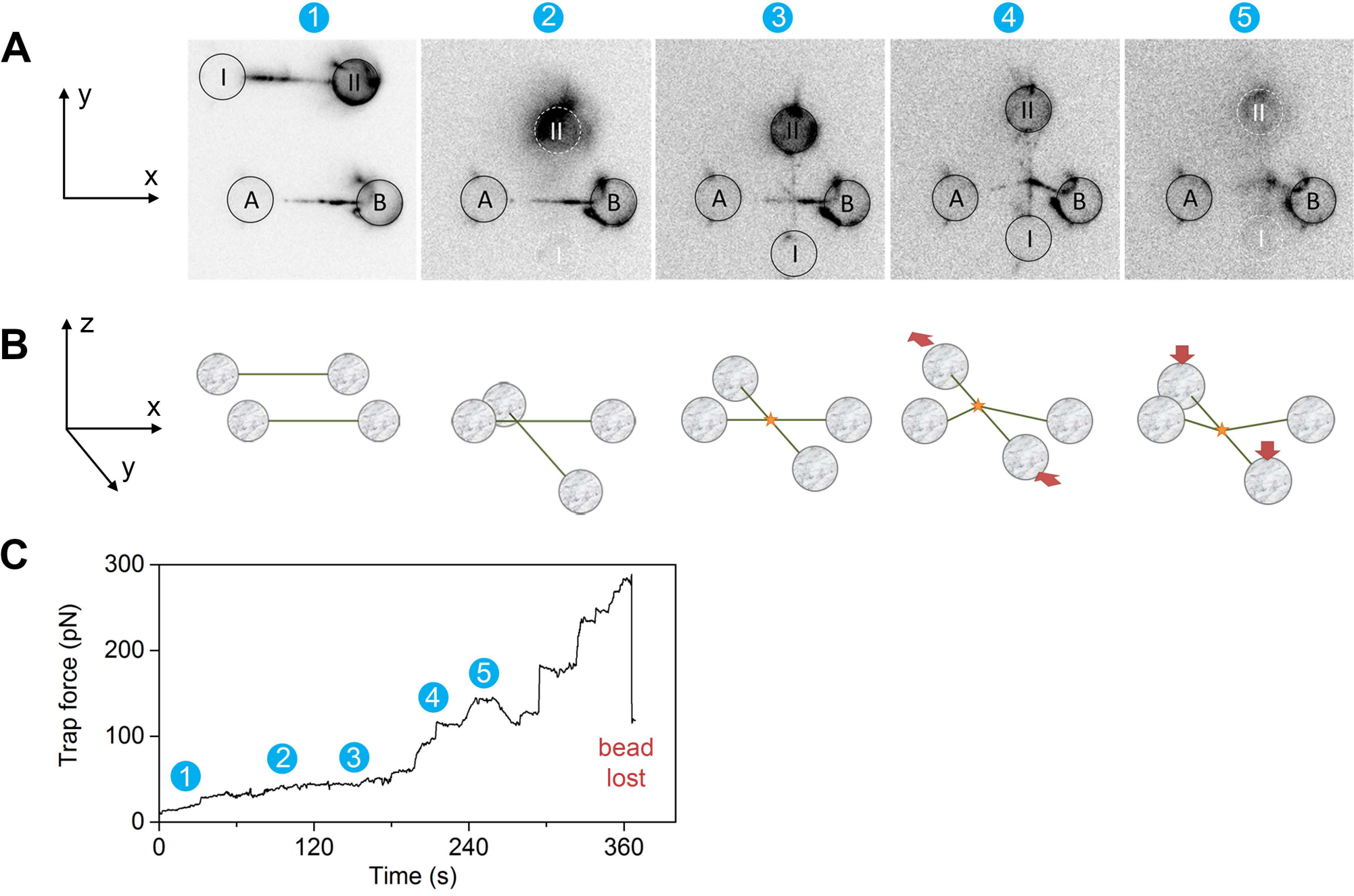
A
1
2
3
4
5
y
x
I
II
A
B
B
z
x
y
C
Trap force (pN)
300
200
100
0
0
120
240
360
Time (s)
bead
lost

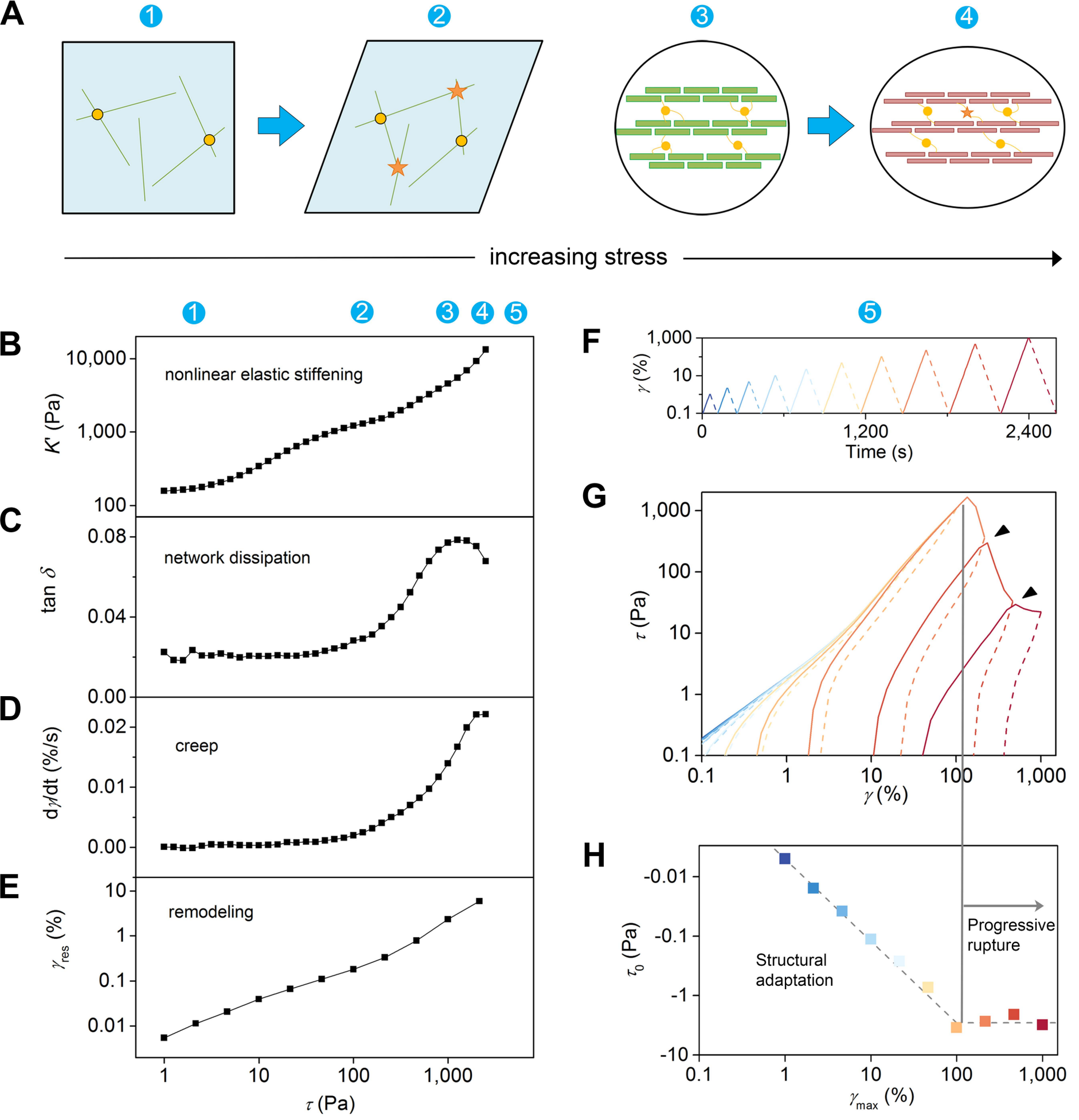
A
1
2
3
4
increasing stress
1
2
3
4
5
B
nonlinear elastic stiffening
K' (Pa)
10,000
1,000
100
C
network dissipation
tan δ
0.08
0.04
0.00
D
creep
dγ/dt (%/s)
0.02
0.01
0.00
E
remodeling
γres (%)
10
1
0.1
0.01
1
10
100
1,000
τ (Pa)
5
F
γ (%)
1,000
10
0.1
0
1,200
2,400
Time (s)
G
1,000
100
10
1
0.1
τ (Pa)
0.1
1
10
100
1,000
γ (%)
H
-0.01
-0.1
-1
-10
τ0 (Pa)
Structural adaptation
Progressive rupture
0.1
1
10
100
1,000
γmax (%)